Adaptive Radar Detection and Range Estimation with Oversampled Data for Partially Homogeneous Environment

C. Hao, *Member, IEEE*, D. Orlando, *Senior Member, IEEE*, G. Foglia, *Member, IEEE*, X. Ma, and C. Hou, *Fellow, IEEE*

***Abstract*—In the present letter we investigate the problem of adaptive detection and range estimation for point-like targets buried in partially homogeneous Gaussian disturbance with unknown covariance matrix. To this end, we jointly exploit the spillover of target energy to consecutive range samples and the oversampling of the received signal. In this context, we design a detector relying on the Generalized Likelihood Ratio Test (GLRT). Remarkably, the new decision scheme ensures the Constant False Alarm Rate (CFAR) property with respect to the unknown disturbance parameters. The performance analysis reveals that it can provide enhanced detection performance compared with its state-of-art counterpart while retaining accurate estimation capabilities of the target position.**

***Index Terms*—Adaptive radar detection, constant false alarm rate, generalized likelihood ratio test, oversampling, partially homogeneous environment.**

I. Introduction

ADAPTIVE radar detection of targets embedded in Gaussian disturbance with unknown spectral properties is a classic task in radar applications, and has received an increasing attention in recent years. Most of the proposed solutions assume a Homogeneous Environment (HE), wherein a set of secondary data free of signal components, but sharing the same spectral properties of the interference in the cells under test (primary data), is available [1]–[7]. However, the HE might not be met in realistic situations: see, for example [7, and references therein]. The most frequently used assumption to depart from a HE is the so-called Partially Homogeneous Environment (PHE), which assumes that primary and secondary data share the same structure of the disturbance covariance matrix but different power levels. Constant False Alarm Rate (CFAR) detection of point-like targets in PHE has been addressed in [9], while CFAR detection of range-spread targets based on the Rao and Wald tests in PHE has been considered in [10]. Other recent solutions can be found in [11]–[17].

The aforementioned detectors, however, are based on the assumption that there is no spillover of the target energy to adjacent matched filter returns. In fact, such assumption is not always reasonable, because there is no guarantee that the samples at the matched filter output is exactly taken at the peak of the target return. The spillover is a physical phenomenon in a radar system and causes a significant loss of signal energy in the above traditional radar signal processing methods. Several methods have been proposed to mitigate or to take advantage of the energy split among adjacent samples. In [18], [19] using two adjacent matched filter samples, it is shown that a monopulse radar may discern up to five targets instead of two by exploiting the spillover. This framework is further generalized in [20] and [21] to the case of Space-Time Adaptive Processing (STAP), wherein a space-time spillover mode for point-like targets is established and three detectors are introduced. These methods accurately estimate the target position within the Cell Under Test (CUT). More recently, in [22] and [23], the oversampling of the noisy returns is used to obtain an adaptive receiver with enhanced detection and localization performance for HE and PHE, respectively.

In the present work, we still deal with the same framework as in [23] and derive an adaptive receiver capable of ensuring better performance than that proposed in [23]. To this end, we first briefly describe the discrete-time model of the oversampled received signal, and then apply the plain GLRT instead of two-step GLRT-based design procedure used in [23], to obtain the decision scheme. The new scheme can exploit the primary data and secondary data more efficiently, due to the fact that the plain GLRT jointly estimate the unknown parameters, while the two-step GLRT separates the estimation of the noise covariance matrix from those of the remaining parameters. Remarkably, the new decision scheme guarantees the CFAR property with respect to the unknown parameters of the disturbance. Finally, we highlight that this letter is a generalization of [21], which refers to the case where the oversampling factor is equal to one and, meantime, is an extension of [22] wherein the plain GLRT for the PHE is not derived. This seemingly minor modification leads to more difficult optimization problems with respect to previous works.

The remainder of the letter is organized as follows. Section II addresses the problem formulation while Section III deals with detector designs. Section IV provides illustrative examples. Finally, Section V contains some concluding remarks.

Manuscript received December 25, 2014; accepted February 12, 2015. Date of publication February 20, 2015; date of current version February 26, 2015. This work was supported by the National Natural Science Foundation of China under Grant 61172166. The associate editor coordinating the review of this manuscript and approving it for publication was Prof. Eric Moreau.

C. Hao, X. Ma and C. Hou are with State Key Laboratory of Acoustics, Institute of Acoustics, Chinese Academy of Sciences, Beijing, China (e-mail: haochengp@mail.ioa.ac.cn; maxc@mail.ioa.ac.cn; hch@mail.ioa.ac.cn).

D. Orlando and G. Foglia are with ELETTRONICA S.p.A., Rome, Italy (e-mail: danilor78@gmail.com; goffredo.foglia@gmail.com).

Color versions of one or more of the figures in this paper are available online at http://ieeexplore.ieee.org.

Digital Object Identifier 10.1109/LSP.2015.2404923

II. Problem Formulation

The aim of this section is to briefly introduce the discrete-time model for the signal and the interference. The interested readers are referred to [23] and [24] for further details. Specifically, the vector of the noisy returns representing the lth range bin is given by

$$\boldsymbol{z}_l^c = \boldsymbol{s}_l + \boldsymbol{n}_l^c \in \mathbb{C}^{N\times 1}, \tag{1}$$

where $N = N_a N_p$ with N_a the number of spatial channels and N_p the number of temporal observations, $\boldsymbol{n}_l^c$ is the interference component with $(\cdot)^c$ the colored matrix or vector, and $\boldsymbol{s}_l$ is the signal component which can be denoted by

$$\boldsymbol{s}_l = \begin{cases} \alpha\chi_p(-(N_s-1)T_p/N_s - \epsilon_0, f)\boldsymbol{v}, & l = l_0 - N_s + 1 \\ \vdots & \vdots \\ \alpha\chi_p(-T_p/N_s - \epsilon_0, f)\boldsymbol{v}, & l = l_0 - 1 \\ \alpha\chi_p(-\epsilon_0, f)v, & l = l_0 \\ \alpha\chi_p(T_p/N_s - \epsilon_0, f)\boldsymbol{v}, & l = l_0 + 1 \\ \vdots & \vdots \\ \alpha\chi_p(T_p - \epsilon_0, f)\boldsymbol{v}, & l = l_0 + N_s \\ 0, & others, \end{cases}$$

with ϵ_0 a residual delay that leads to target energy spillover, f the target Doppler frequency, $N_s \in \mathbb{N}$ the oversampling factor, l_0 the sample under test, T_p the duration of transmitted pulse, $\chi_p(\cdot,\cdot)$ the complex ambiguity function of the transmitted pulse waveform, and $\boldsymbol{v}$ the space-time steering vector[1].

Alternatively, we define the residual delay, ϵ say, evaluated with respect to the lth range bin accounting for the target positions surrounding the considered bin center as follows

$$\epsilon = \begin{cases} \epsilon_0, & \text{if } l = l_0 \text{ and } 0 \le \epsilon_0 \le \frac{T_p}{2N_s}, \\ \epsilon_0 - \frac{T_p}{N_s}, & \text{if } l = l_0 + 1 \text{ and } \frac{T_p}{2N_s} < \epsilon_0 \le \frac{T_p}{N_s}. \end{cases} \tag{2}$$

As pointed in [23], although the oversampling makes interference samples spatially correlated with a correlation tied up to the waveform ambiguity function, it is possible to show that the structure of the fast-time interference correlation is functionally independent of the environmental parameters under reasonable technical assumptions. Therefore, a whitening matrix $\boldsymbol{W}$ can be pre-canned into the system and used to spatially decorrelate primary data. The whitened primary data matrix can be written as [23]

$$\boldsymbol{Z}_P = \boldsymbol{Z}_P^c \boldsymbol{W} = [\boldsymbol{z}_{l-N_s}, \ldots, \boldsymbol{z}_l, \ldots, \boldsymbol{z}_{l+N_s}], \tag{3}$$

where $\boldsymbol{Z}_P^c = [\boldsymbol{z}_{l-N_s}^c, \ldots, \boldsymbol{z}_l^c, \ldots, \boldsymbol{z}_{l+N_s}^c]$, and

$$\boldsymbol{W} = \begin{bmatrix} w_{-N_s,-N_s} & \cdots & w_{-N_s,N_s} \\ \vdots & \ddots & \vdots \\ w_{N_s,-N_s} & \cdots & w_{N_s,N_s} \end{bmatrix} \in \mathbb{C}^{(2N_s+1)\times(2N_s+1)}.$$

As customary, we assume that a secondary dataset $\boldsymbol{Z}_K^c$, free of signal components, is available. Precisely, $\boldsymbol{Z}_K^c$ are chosen from a set of adjacent range cells of primary data, and given by $\boldsymbol{Z}_K^c = [\boldsymbol{z}_{k_1}^c, \ldots, \boldsymbol{z}_{k_K}^c]$, where the indices $k_1, \ldots, k_K$ account for a guard interval, and $K \ge N$. Following the same line of reasoning as for the primary data, the whitened secondary data matrix can be written as $\boldsymbol{Z}_K = [\boldsymbol{z}_{k_1}, \ldots, \boldsymbol{z}_{k_K}]$. Summarizing, the decision problem can be formulated as a binary hypothesis testing problem

[1]For the sake of brevity we omit the dependence of $\boldsymbol{v}$ on the spatial and the Doppler frequency.

$$\begin{cases} H_0 : \begin{cases} \boldsymbol{z}_i = \boldsymbol{n}_i, & i = l - N_s, \ldots, l + N_s, \\ \boldsymbol{z}_k = \boldsymbol{n}_k, & k = k_1, \ldots, k_K, \end{cases} \\ H_1 : \begin{cases} \boldsymbol{z}_i = \alpha\mathcal{F}_i(\epsilon, \boldsymbol{W})\boldsymbol{v} + \boldsymbol{n}_i, & i = l - N_s, \ldots, l + N_s, \\ \boldsymbol{z}_k = \boldsymbol{n}_k, & k = k_1, \ldots, k_K, \end{cases} \end{cases} \tag{4}$$

where α is unknown deterministic factors which account for both target reflectivity and channel effects, $\boldsymbol{n}_i, i = l - N_s, \ldots, l + N_s$, and $\boldsymbol{n}_k$, $k = k_1, \ldots, k_K$, are independent complex normal random vectors with zero mean and covariance matrices $E[\boldsymbol{n}_i\boldsymbol{n}_i^\dagger] = \gamma\boldsymbol{M}$ and $E[\boldsymbol{n}_k\boldsymbol{n}_k^\dagger] = \boldsymbol{M}$, with $\gamma > 0$ the power scaling factor, and † the conjugate transpose. Finally, $\mathcal{F}_i(\epsilon, \boldsymbol{W})$ is given by $\sum_{m=-N_s}^{N_s} w_{m,i-l}\chi_p(mT_p/N_s - \epsilon, f)$ with $-T_p/(2N_s) \le \epsilon \le T_p/(2N_s)$, and $i = l - N_s, \ldots, l + N_s$.

III. Detector Design

In this section, we solve problem (4) resorting to the GLRT. To begin with, let us denote by $L = 2N_s + 1$, $\boldsymbol{Z} = [\boldsymbol{Z}_P\ \boldsymbol{Z}_K] \in \mathbb{C}^{N\times(L+K)}$ the overall data matrix, and $\mathcal{F}(\epsilon) = [\mathcal{F}_{l-N_s}(\epsilon, \boldsymbol{W}), \mathcal{F}_{l-N_s+1}(\epsilon, \boldsymbol{W}), \ldots, \mathcal{F}_{l+N_s}(\epsilon, \boldsymbol{W})]^T$. The GLRT based on primary and secondary data is given by

$$\frac{\max_{\epsilon,\gamma,\alpha,\mathbf{M}} f_1(\boldsymbol{Z}; \boldsymbol{M}, \gamma, \alpha, \epsilon)}{\max_{\gamma,\mathbf{M}} f_0(\boldsymbol{Z}; \boldsymbol{M}, \gamma, 0, 0)} \underset{H_0}{\overset{H_1}{\gtrless}} \eta, \tag{5}$$

where η is the threshold to be set according to the desired Probability of False Alarm (P_{fa}), and $f_i(\boldsymbol{Z}; \cdot)$ is the Probability Density Function (PDF) of $\boldsymbol{Z}$ under H_i, $i = 0, 1$, namely

$$f_i(\boldsymbol{Z}; \boldsymbol{M}, \gamma, i\alpha, i\epsilon) = \left[\frac{\exp\left\{-\text{tr}\left[\boldsymbol{M}^{-1}\left(\frac{1}{\gamma}\boldsymbol{p}_i\boldsymbol{p}_i^\dagger + \boldsymbol{S}\right)\right]\right\}}{\pi^N\gamma^{\frac{LN}{K+L}}\det(\boldsymbol{M})}\right]^{K+L}, \tag{6}$$

In (6), $\boldsymbol{p}_i = \boldsymbol{Z}_P - i\alpha\boldsymbol{v}\mathcal{F}^T(\epsilon)$, $\boldsymbol{S} = \boldsymbol{Z}_K\boldsymbol{Z}_K^\dagger$ is the K times sample covariance matrix of the secondary data, $\det(\cdot)$ and $\text{tr}(\cdot)$ denote the determinant and the trace of a square matrix, respectively. Let us focus on the optimization problem under H_1 firstly. It is well known that the maximum likelihood estimate of $\boldsymbol{M}$, $\widehat{\boldsymbol{M}}$ say, is given by the sample covariance matrix. Replacing $\boldsymbol{M}$ with $\widehat{\boldsymbol{M}}$ yields

$$f_1(\boldsymbol{Z}; \widehat{\boldsymbol{M}}, \gamma, \alpha, \epsilon) \propto \left[\gamma^{\frac{LN}{K+L}}\det\left(\frac{1}{\gamma}\boldsymbol{p}_1\boldsymbol{p}_1^\dagger + \boldsymbol{S}\right)\right]^{-(K+L)}, \tag{7}$$

where $\propto$ denotes proportional to. Now maximization with respect to α is tantamount to $\min_\alpha \det[\frac{1}{\gamma}\boldsymbol{p}_1\boldsymbol{p}_1^\dagger + \boldsymbol{S}]$, where the argument can be recast as follows

$$\begin{aligned} &\det\left[\frac{1}{\gamma}\boldsymbol{p}_1\boldsymbol{p}_1^\dagger + \boldsymbol{S}\right] = \det[\boldsymbol{S}]\det\left[\boldsymbol{I}_L + \frac{1}{\gamma}\boldsymbol{p}_1^\dagger\boldsymbol{S}^{-1}\boldsymbol{p}_1\right] \\ &= \det[\boldsymbol{S}]\gamma^{-L}\det\left[\gamma\boldsymbol{I}_L + \boldsymbol{p}_1^\dagger\boldsymbol{S}^{-1/2}\left(\boldsymbol{P}_{\boldsymbol{v}_s}^\perp + \boldsymbol{P}_{\boldsymbol{v}_s}\right)\boldsymbol{S}^{-1/2}\boldsymbol{p}_1\right] \\ &= \frac{\det[\gamma\boldsymbol{I}_L + \boldsymbol{A}]}{\det[\boldsymbol{S}]^{-1}\gamma^L}\left[1 + \frac{\boldsymbol{v}^\dagger\boldsymbol{S}^{-1}\boldsymbol{p}_1(\gamma\boldsymbol{I}_L + \boldsymbol{A})^{-1}\boldsymbol{p}_1^\dagger\boldsymbol{S}^{-1}\boldsymbol{v}}{\boldsymbol{v}^\dagger\boldsymbol{S}^{-1}\boldsymbol{v}}\right] \end{aligned} \tag{8}$$

with $\boldsymbol{I}_N$ the N-dimensional identity matrix, $\boldsymbol{P}_{\boldsymbol{v}_s} = \boldsymbol{v}_s(\boldsymbol{v}_s^H\boldsymbol{v}_s)^{-1}\boldsymbol{v}_s^H$ the projection matrix onto the subspace spanned by $\boldsymbol{v}_s = \boldsymbol{S}^{-1/2}\boldsymbol{v}$, $\boldsymbol{P}_{\boldsymbol{v}_s}^\perp = \boldsymbol{I}_N - \boldsymbol{P}_{\boldsymbol{v}_s}$, and $\boldsymbol{A} = \boldsymbol{Z}_P^H\boldsymbol{S}^{-1/2}\boldsymbol{P}_{\boldsymbol{v}_s}^\perp\boldsymbol{S}^{-1/2}\boldsymbol{Z}_P$. The last equality comes from $\det(\boldsymbol{I}_L + \boldsymbol{u}\boldsymbol{u}^\dagger) = 1 + \boldsymbol{u}^\dagger\boldsymbol{u}$ with $\boldsymbol{u} \in \mathbb{C}^{L\times 1}$. Thus, the optimization problem with respect to α is equivalent to

$\min_{\alpha} \boldsymbol{v}^\dagger \boldsymbol{S}^{-1} p_1(\gamma \boldsymbol{I}_L + \boldsymbol{A})^{-1} \boldsymbol{p}_1^\dagger \boldsymbol{S}^{-1} \boldsymbol{v}$. Setting to zero the derivative with respect to α, yields [22]

$$\widehat{\alpha} = \frac{\boldsymbol{v}^\dagger \boldsymbol{S}^{-1} \boldsymbol{Z}_P (\gamma \boldsymbol{I}_L + \boldsymbol{A})^{-1} \mathcal{F}^*(\epsilon)}{\mathcal{F}^T(\epsilon)(\gamma \boldsymbol{I}_L + \boldsymbol{A})^{-1} \mathcal{F}^*(\epsilon) \boldsymbol{v}^\dagger \boldsymbol{S}^{-1} \boldsymbol{v}} = \frac{\widehat{\alpha}_{No}}{\widehat{\alpha}_{De}}, \quad (9)$$

where * denotes complex conjugate. It follows that

$$\begin{aligned} &\min_{\alpha} \boldsymbol{v}^\dagger \boldsymbol{S}^{-1} \boldsymbol{p}_1 (\gamma \boldsymbol{I}_L + \boldsymbol{A})^{-1} \boldsymbol{p}_1^\dagger \boldsymbol{S}^{-1} \boldsymbol{v} \\ &= \boldsymbol{v}^\dagger \boldsymbol{S}^{-1} \boldsymbol{Z}_P (\gamma \boldsymbol{I}_L + \boldsymbol{A})^{-1} \boldsymbol{Z}_P^\dagger \boldsymbol{S}^{-1} \boldsymbol{v} - \frac{(\boldsymbol{v}^\dagger \boldsymbol{S}^{-1} \boldsymbol{v}) |\widehat{\alpha}_{No}|^2}{\widehat{\alpha}_{De}} \end{aligned} \quad (10)$$

Based on the results in (8) and (10), we have

$$\begin{aligned} f_1(\boldsymbol{Z}; \widehat{\boldsymbol{M}}, \gamma, \widehat{\alpha}, \epsilon) \propto &\left[\gamma^{\frac{LN}{K+L} - L} \det(\gamma \boldsymbol{I}_L + \boldsymbol{A}) \right]^{-(K+L)} \\ &\times \left(1 + \frac{\boldsymbol{v}^\dagger \boldsymbol{S}^{-1} \boldsymbol{Z}_P (\gamma \boldsymbol{I}_L + \boldsymbol{A})^{-1} \boldsymbol{Z}_P^\dagger \boldsymbol{S}^{-1} \boldsymbol{v}}{\boldsymbol{v}^\dagger \boldsymbol{S}^{-1} \boldsymbol{v}} - \frac{|\widehat{\alpha}_{No}|^2}{\widehat{\alpha}_{De}} \right)^{-(K+L)}. \end{aligned} \quad (11)$$

Observe that the eigendecomposition of $\boldsymbol{A}$ is $\boldsymbol{A} = \boldsymbol{U} \boldsymbol{\Lambda} \boldsymbol{U}^\dagger$, where $\boldsymbol{\Lambda}$ is a diagonal matrix containing the eigenvalues of $\boldsymbol{A}$, i.e., $\boldsymbol{\Lambda} = diag\{\lambda_1, \ldots, \lambda_L\}$, and $\boldsymbol{U}$ is a unitary matrix. Moreover, let us define symbols that will come in handy for the optimization with respect to γ, namely, $\boldsymbol{v}_u = (\boldsymbol{v}^\dagger \boldsymbol{S}^{-1} \boldsymbol{v})^{-1/2} \boldsymbol{U}^\dagger \boldsymbol{Z}_P^\dagger \boldsymbol{S}^{-1} \boldsymbol{v} = [v_1, \ldots, v_L]^T$, and $\mathcal{F}_u = \boldsymbol{U}^\dagger \mathcal{F}^*(\epsilon) = [F_1, \ldots, F_L]^T$. It follows that the $(K+L)$th root of the denominator of (11) can be recast as

$$\begin{aligned} f(\gamma) &= \gamma^m \prod_{i \in \Omega} (\gamma + \lambda_i) \left(1 + \sum_{i \in \Omega} \frac{b_i}{\gamma + \lambda_i} - \frac{\sum_{i \in \Omega} c_i / (\gamma + \lambda_i)}{\sum_{i \in \Omega} a_i / (\gamma + \lambda_i)} \right) \\ &= \gamma^m \left(h(\gamma) + \sum_{i \in \Omega} b_i p_i(\gamma) - \frac{\left| \sum_{i \in \Omega} c_i p_i(\gamma) \right|^2}{\sum_{i \in \Omega} a_i p_i(\gamma)} \right), \end{aligned} \quad (12)$$

where $m = \frac{LN}{K+L} - L$, $a_i = |F_i|^2$, $b_i = |v_i|^2$, $c_i = v_i^* F_i$, $h(\gamma) = \prod_{i \in \Omega} (\gamma + \lambda_i)$, and $p_i(\gamma) = \prod_{j \in \Omega, j \neq i} (\gamma + \lambda_j)$, $i \in \Omega \equiv \{1, \ldots, L\}$. Observe that $f(\gamma)$ is a continuous on $(0, \infty)$, and[2]

$$\lim_{\gamma \to 0} f(\gamma) = +\infty, \text{ if } K + L > N \ (m < 0), \quad (13)$$

$$\lim_{\gamma \to +\infty} f(\gamma) = +\infty, \text{ if } m + L > 0 \ (N > 0). \quad (14)$$

The above equalities ensure that at least a minimum exists. For this reason, we search the absolute minimum between the positive solutions of the equation $df(\gamma)/d\gamma = 0$, which is differentiable in $(0, +\infty)$. It is easy to show that $dh(\gamma)/d\gamma = \sum_{i \in \Omega} p_i(\gamma)$, $dp_i(\gamma)/d\gamma = q_i(\gamma)$, and $d|\sum_{i \in \Omega} c_i p_i(\gamma)|^2 / d\gamma = 2\mathrm{Re}[\sum_{i \in \Omega} c_i p_i(\gamma) \sum_{i \in \Omega} c_i^* q_i(\gamma)]$ with $q_i(\gamma) = \sum_{j \in \Omega, j \neq i} \prod_{k \in \Omega, k \neq i, j} (\gamma + \lambda_k)$, and $Re(\cdot)$ the real part of the argument. Hence, $df(\gamma)/d\gamma = 0$ can be expressed as

$$\begin{aligned} &\left(\gamma \left[\sum_{i \in \Omega} p_i(\gamma) + \sum_{i \in \Omega} b_i q_i(\gamma) \right] + m \left[h(\gamma) + \sum_{i \in \Omega} b_i p_i(\gamma) \right] \right) x^2(\gamma) \\ &+ \left(m \left| \sum_{i \in \Omega} c_i p_i(\gamma) \right|^2 - 2\gamma Re \left[\sum_{i \in \Omega} c_i p_i(\gamma) \sum_{i \in \Omega} c_i^* q_i(\gamma) \right] \right) x(\gamma) \\ &+ \gamma \left| \sum_{i \in \Omega} c_i p_i(\gamma) \right|^2 \sum_{i \in \Omega} a_i q_i(\gamma) = 0, \end{aligned} \quad (15)$$

[2]Recall that $K \geq N > 0$.

where $x(\gamma) = \sum_{i \in \Omega} a_i p_i(\gamma)$. It is easy to know that the degree of (15) is $6N_s + 1 \geq 7$, and hence, we have to solve it resorting to numerical algorithms such as the Newton-Raphson or Laguerre methods. Anyway, we can obtain $\widehat{\gamma}_1$ by using standard numerical routines such as '*fzero*' of Matlab.

Similarly, the compressed likelihood under H_0 is given by

$$f_0(\boldsymbol{Z}; \widehat{\boldsymbol{M}}, \gamma, 0, 0) \propto \left[\gamma^m \prod_{i \in \Omega} (\gamma + \mu_i) \right]^{-(K+L)}, \quad (16)$$

where μ_i, $i \in \Omega$, are the eigenvalues of $\boldsymbol{Z}_P^\dagger \boldsymbol{S}^{-1} \boldsymbol{Z}_P$. According to Proposition 2 of [25], it is easy to show that the RHS of (16) attains its absolute minimum $\widehat{\gamma}_0$ (if $K + L > N$) at the unique positive solution of the equation,

$$m g(\gamma) + \gamma \sum_{i \in \Omega} y_i(\gamma) = 0, \quad (17)$$

where $g(\gamma) = \prod_{i \in \Omega} (\gamma + \mu_i)$, and $y_i(\gamma) = \prod_{j \in \Omega, j \neq i} (\gamma + \mu_j)$, $i \in \Omega$. Note that the degree of the above equation is $2N_s + 1 \geq 3$, and it can be solved by using the Matlab function '*fzero*'.

Gathering the above results, the GLRT can be recast as

$$\max_{\epsilon \in \left[-\frac{T_p}{2N_s}, \frac{T_p}{2N_s} \right]} \frac{\widehat{\gamma}_0^{\frac{LN}{K+L}} \det\left[\frac{1}{\widehat{\gamma}_0} \boldsymbol{Z}_P \boldsymbol{Z}_P^\dagger + \boldsymbol{S} \right]}{\widehat{\gamma}_1^{\frac{LN}{K+L}} \det\left[\frac{1}{\widehat{\gamma}_1} \widehat{\boldsymbol{p}}_1 \widehat{\boldsymbol{p}}_1^\dagger + \boldsymbol{S} \right]} \underset{H_0}{\overset{H_1}{\gtrless}} \eta, \quad (18)$$

where $\widehat{\boldsymbol{p}}_1 = \boldsymbol{Z}_P - \widehat{\alpha} \boldsymbol{v} \mathcal{F}^T(\epsilon)$.

As a final remark, it is difficult to obtain a closed-form estimate of ϵ, and, hence we resort to a grid search to perform the maximization with respect to ϵ. The grid-search-based implementation of (18) will be referred to in the sequel as the Oversampled GLRT for PHE (OS-GLRT-PHE). Moreover, the new receiver ensures the CFAR property with respect to M and γ. Proof of such statements, not reported here for the sake of brevity, follows the lead of [20] and references therein.

Finally, the implementation of the OS-GLRT-PHE requires solving (15) and (17) under H_1 and H_0, respectively and hence, an additional processing cost with respect to the so-called Oversampled ACE (OS-ACE) derived in [23].

IV. Performance Assessment

This section is devoted to the performance assessment of the proposed detection algorithms in terms of Probability of Detection (P_d) and Root Mean Square (RMS) errors in range. To this end, we compare the proposed detector with OS-ACE.

We make use of standard Monte Carlo counting techniques and evaluate the thresholds necessary to ensure a preassigned value of P_fa resorting to $100/P_{fa}$ independent trials. The P_d values and the RMS range errors are estimated over 10^4 and 10^3 independent trials, respectively. All the illustrative examples assume $P_{fa} = 10^{-4}$, $f_c = 10^9$ Hz, $T_p = 0.2$ μs, $c = 3 \cdot 10^8$ m/s, and $f = 0$. The actual position of the target is assumed (independent from trial to trial) uniformly distributed in $(t_{\min} + (l-1)T_p - T_p/(2N_s), t_{\min} + (l-1)T_p + T_p/(2N_s))$. As to ϵ, it takes on values in $\{\frac{n - N_\epsilon}{2N_\epsilon} \frac{T_p}{N_s}\}_{n=0}^{2N_\epsilon}$ with $N_\epsilon = 5$. The interference is modeled as a complex normal vector with the space-time covariance matrix $\boldsymbol{M} = \sigma_n^2 \boldsymbol{I}_N + \sigma_c^2 \boldsymbol{M}_c$, where $\sigma_n^2 = 1$, $\sigma_c^2 > 0$ is evaluated assuming a clutter-to-noise ratio of 30 dB, the (i,j)th element of $\boldsymbol{M}_c$ is given by $\rho^{|i-j|}$ with $\rho = 0.9$ [26], [27]. Finally, the SNR is defined as $SNR = \frac{|\alpha|^2}{\gamma} \boldsymbol{v}^\dagger \boldsymbol{M}^{-1} \boldsymbol{v} \sum_{i=l-N_s}^{l+N_s} |\mathcal{F}_i(\epsilon, \boldsymbol{W})|^2$.

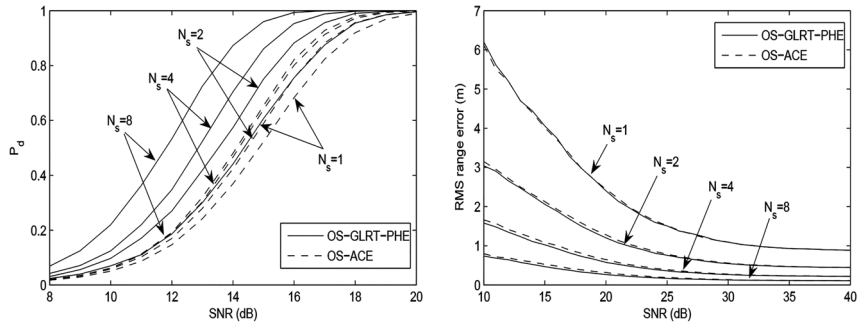

Fig. 1. Performance of the OS-GLRT-PHE and OS-ACE with simulated data; $N = N_a = 8$, $K = 16$, $N_\epsilon = 5$, $\gamma = 5$, and $P_{fa} = 10^{-4}$.

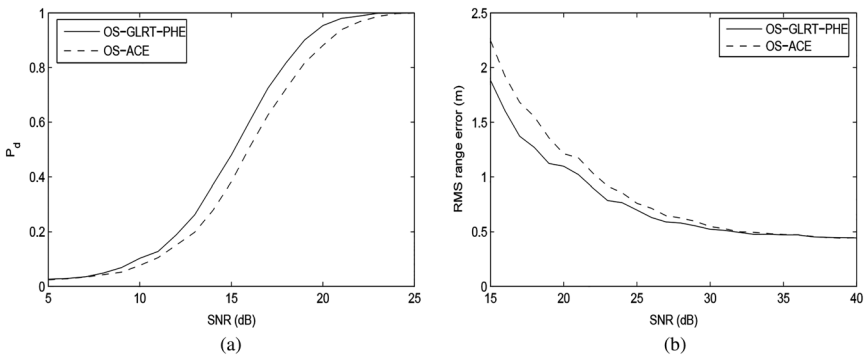

Fig. 2. Performance of the OS-GLRT-PHE and OS-ACE with real data; $N = N_a = 8$, $K = 16$, $N_\epsilon = 5$, $\gamma = 5$, and $P_{fa} = 10^{-4}$.

In Fig. 1, we study the performance of the OS-GLRT-PHE assuming $N = N_a = 8$, $K = 16$, $\gamma = 5$, and N_s as parameter. More precisely, in Fig. 1(a) we plot P_d versus SNR, whereas in Fig. 1(b) the comparisons are in terms of RMS errors in range. As it can be seen from Fig. 1, the GLRT-LC-PHE guarantees a superior detection performance than the OS-ACE. Moreover, the greater N_s, the higher the detection gains of the OS-GLRT-PHE with respect to the OS-ACE. On the other hand, the curves reported in Fig. 1b show that the two receivers have practically the same RMS errors. All above results show that oversampling is a suitable means to enhance radar system performance even when a scale mismatch between primary and secondary data is present. It is worth noting that for high SNR values, the RMS errors become identical, because they achieve the lower bound given by the grid resolution $\Delta = T_p/(2N_\epsilon)$.

In order to show the performance of the OS-GLRT-PHE in a realistic environment, we exploit the real radar measurements collected using the McMaster IPIX radar from a site in Dartmouth. Our analysis refers to the file 19931117 131609 stareB0002.cdf (dataset 226 of [28]). The details on the experiment can be found in [28]. Since the real data were oversampled with a factor equal to 2, we only consider the case of $N_s = 2$. We use the range cells 48-52 of VV channel as the primary data, and the range cells adjacent to the primary data as the secondary data; specifically, we choose the range cells 39-46 and 54-61 for $K = 16$. The performance of the OS-GLRT-PHE and the OS-ACE are evaluated under the same number of False Alarms (FA). This is because the limited amount of real data do not allow a Monte Carlo estimation of the P_{fa}. Precisely, we set $FA = 15$, which corresponds to an obtained P_{fa} of about 10^{-2}. Note that the dataset 226 entails only clutter and that a synthetic target is injected at the zero velocity with a given SNR and residual delay. Moreover, the SNR is defined as $SNR = |\alpha|^2 \boldsymbol{v}^H \widetilde{\boldsymbol{M}}^{-1} \boldsymbol{v}$, where $\widetilde{\boldsymbol{M}}$ is the estimated sample covariance matrix using all the returns of the range cells 48-52. As to the residual delay, it randomly and uniformly distributed over $(-T_p/2N_s, T_p/2N_s)$.

The corresponding results are shown in Fig. 2 in terms of $P_{\rm d}$ versus SNR and RMS errors versus SNR assuming $N = N_p = 8$ and $K = 16$. Inspection of the figure confirms the trend observed on simulated data, namely that the OS-GLRT-PHE ensures better detection performance then the OS-ACE. Finally, it is worth noting that in HE the OS-GLRT-PHE and OS-ACE would suffer a P_d loss with respect to their counterparts devised for HE [22], due to the fact that they are scale-invariant to the power scaling factor γ.

V. Conclusions

In this work, we have proposed an adaptive decision scheme with enhanced detection and range estimation capabilities for point-like targets in partially homogeneous Gaussian disturbance. For the sake of deriving the new detector, we jointly take advantage of the oversampling of the noisy returns as well as the target energy spillover to adjacent range samples, and resort to the plain GLRT. Notably, the OS-GLRT-PHE possesses the CFAR property with respect to with respect to both the structure of the covariance matrix as well as the power level. The performance assessment, conducted on both simulated data and real recorded data, has shown that the OS-GLRT-PHE can guarantee better detection performance than the OS-ACE. As to the range estimation capabilities, the OS-GLRT-PHE is comparable to the OS-ACE. Possible research could concern the problem of detection and range estimation for non-Gaussian scenarios [29]–[31].

REFERENCES

[1] E. J. Kelly, "An adaptive detection algorithm," *IEEE Trans. Aerosp. Electron. Syst.*, vol. 22, no. 2, pp. 115–127, Mar. 1986.

[2] F. C. Robey, D. L. Fuhrman, E. J. Kelly, and R. Nitzberg, "A CFAR adaptive matched filter detector," *IEEE Trans. Aerosp. Electron. Syst.*, vol. 29, no. 1, pp. 208–216, Jan. 1992.

[3] C. D. Richmond, "Performance of the adaptive sidelobe blanker detection algorithm in homogeneous environments," *IEEE Trans. Signal Process.*, vol. 48, no. 5, pp. 1235–1247, May 2000.

[4] S. D. Blunt and K. Gerlach, "Efficient robust AMF using the FRACTA algorithm," *IEEE Trans. Aerosp. Electron. Syst.*, vol. 41, no. 2, pp. 537–548, Apr. 2005.

[5] K. Sohn, H. Li, and B. Himed, "Parametric GLRT for multichannel adaptive signal detection," *IEEE Trans. Signal Process.*, vol. 55, no. 11, pp. 5351–5360, Nov. 2007.

[6] A. Aubry, A. De Maio, D. Orlando, and M. Piezzo, "Adaptive detection of point-like targets in the presence of homogeneous clutter and subspace interference," *IEEE Signal Process. Lett.*, vol. 21, no. 7, pp. 848–852, Jul. 2014.

[7] W. Liu, W. Xie, J. Liu, and Y. Wang, "Adaptive double subspace signal detection in gaussian fbackground-part I: Homogeneous environments," *IEEE Trans. Signal Process.*, vol. 62, no. 9, pp. 2345–2357, Sep. 2014.

[8] W. L. Melvin, "Space-time adaptive radar performance in heterogeneous clutter," *IEEE Trans. Aerosp. Electron. Syst.*, vol. 36, no. 2, pp. 621–633, Apr. 2000.

[9] S. Kraut and L. L. Scharf, "The CFAR adaptive subspace detector is a scale-invariant GLRT," *IEEE Trans. Signal Process.*, vol. 47, no. 9, pp. 2538–2541, Sep. 1999.

[10] C. Hao, X. Ma, X. Shang, and L. Cai, "Adaptive detection of distributed targets in partially homogeneous environment with rao and wald tests," *Signal Process.*, vol. 92, no. 4, pp. 926–930, Apr. 2012.

[11] A. De Maio and S. Iommelli, "Coincidence of the Rao test, wald test, and GLRT in partially homogeneous environment," *IEEE Signal Process. Lett.*, vol. 15, pp. 385–388, 2008.

[12] F. Bandiera, A. De Maio, A. S. Greco, and G. Ricci, "Adaptive radar detection of distributed targets in homogeneous and partially homogeneous noise plus subspace interference," *IEEE Trans. Signal Process.*, vol. 55, no. 4, pp. 1223–1237, Apr. 2007.

[13] S. Bidon, O. Besson, and J. Y. Tourneret, "The adaptive coherence estimator is the generalized likelihood ratio test for a class of heterogeneous environments," *IEEE Signal Process. Lett.*, vol. 15, pp. 281–284, 2008.

[14] J. Liu, Z. Zhang, Y. Yang, and H. Liu, "A CFAR adaptive subspace detector for first-order or second-order gaussian signals based on a single observation," *IEEE Trans. Signal Process.*, vol. 59, no. 11, pp. 5126–5140, Nov. 2011.

[15] P. Wang, H. Li, and B. Himed, "Parametric rao tests for multichannel adaptive detection in partially homogeneous environment," *IEEE Trans. Aerosp. Electron. Syst.*, vol. 47, no. 3, pp. 1850–1862, Jul. 2011.

[16] W. Liu, W. Xie, J. Liu, and Y. Wang, "Adaptive double subspace signal detection in gaussian background part II: Partially homogeneous environments," *IEEE Trans. Signal Process.*, vol. 62, no. 9, pp. 2358–2369, Sep. 2014.

[17] Y. Gao, G. Liao, S. Zhu, X. Zhang, and D. Yang, "Persymmetric adaptive detectors in homogeneous and partially homogeneous environments," *IEEE Trans. Signal Process.*, vol. 62, no. 2, pp. 331–342, Feb. 2014.

[18] X. Zhang, P. K. Willett, and Y. Bar-Shalom, "Monopulse radar detection and localization of multiple unresolved targets via joint bin processing," *IEEE Trans. Signal Process.*, vol. 53, no. 4, pp. 1225–1236, Apr. 2005.

[19] X. Zhang, P. K. Willett, and Y. Bar-Shalom, "Detection and localization of multiple unresolved extended targets via monopulse radar signal processing," *IEEE Trans. Aerosp. Electron. Syst.*, vol. 45, no. 2, pp. 455–472, Apr. 2009.

[20] D. Orlando and G. Ricci, "Adaptive radar detection and localization of a point-like target," *IEEE Trans. Signal Process.*, vol. 59, no. 9, pp. 4086–4096, Sep. 2011.

[21] A. De Maio, C. Hao, and D. Orlando, "An adaptive detector with range estimation capabilities for partially homogeneous environment," *IEEE Signal Process. Lett.*, vol. 21, no. 3, pp. 325–329, Mar. 2014.

[22] A. Aubry, A. De Maio, G. Foglia, C. Hao, and D. Orlando, "Radar detection and range estimation using oversampled data," *IEEE Trans. Aerosp. Electron. Syst.*, to be published.

[23] A. Aubry, A. De Maio, G. Foglia, C. Hao, and D. Orlando, "A radar detector with enhanced range estimation capabilities for partially homogeneous environment," *IET Radar, Sonar Navig.*, vol. 48, no. 9, pp. 1018–1025, Dec. 2014.

[24] F. Bandiera, D. Orlando, and G. Ricci, "Advanced radar detection schemes under mismatched signal models," in *Synthesis Lectures on Signal Processing*. San Rafael, CA, USA: Morgan & Claypool, 2009, 8.

[25] E. Conte, A. De Maio, and G. Ricci, "GLRT-based adaptive detection algorithms for range-spread targets," *IEEE Trans. Signal Process.*, vol. 49, no. 7, pp. 1336–1348, Jul. 2001.

[26] E. Conte, A. De Maio, and C. Galdi, "Statistical analysis of real clutter at different range resolutions," *IEEE Trans. Aerosp. Electron. Syst.*, vol. 40, no. 3, pp. 903–918, Jul. 2004.

[27] E. Conte, A. De Maio, and A. Farina, "Statistical tests for higher order analysis of radar clutter: Their application to l-band measured data," *IEEE Trans. Aerosp. Electron. Syst.*, vol. 41, no. 1, pp. 205–218, Jan. 2005.

[28] [Online]. Available: http://soma.crl.mcmaster.ca/ipix/

[29] S. Watts, "Radar detection prediction in K-distributed sea clutter and thermal noise," *IEEE Trans. Aerosp. Electron. Syst.*, vol. AES-23, no. 1, pp. 40–45, Jan. 1987.

[30] F. Gini and A. Farina, "Vector subspace detection in compound-gaussian clutter part i: Survey and new results," *IEEE Trans. Aerosp. Electron. Syst.*, vol. 38, no. 4, pp. 1295–1311, Oct. 2002.

[31] F. Gini and M. Greco, "Suboptimum approach to adaptive coherent radar detection in compound-gaussian clutter," *IEEE Trans. Aerosp. Electron. Syst.*, vol. 35, no. 3, pp. 1095–1103, Jul. 1999.